

## Purcell-Enhanced Spontaneous Emission of Molecular Vibrations

Bernd Metzger,<sup>1</sup> Eric Muller,<sup>1</sup> Jun Nishida,<sup>1</sup> Benjamin Pollard,<sup>1</sup> Mario Hentschel,<sup>2</sup> and Markus B. Raschke<sup>1,\*</sup>

<sup>1</sup>*Department of Physics, Department of Chemistry, and JILA, University of Colorado at Boulder, Colorado 80309, USA*

<sup>2</sup>*4th Physics Institute and Research Center SCoPE, University of Stuttgart, Pfaffenwaldring 57, 70569 Stuttgart, Germany*



(Received 25 February 2019; revised manuscript received 24 June 2019; published 10 October 2019)

Infrared (IR) spectroscopy of molecular vibrations provides insight into molecular structure, coupling, and dynamics. However, picosecond scale intermolecular and intramolecular many-body interactions, nonradiative relaxation, absorption, and thermalization typically dominate over IR spontaneous emission. We demonstrate how coupling to a resonant IR antenna can enhance spontaneous emission of molecular vibrations. Using time-domain nanoprobe spectroscopy we observe an up to 50% decrease in vibrational dephasing time  $T_{2,\text{vib}}$ , based on the coupling-induced population decay with  $T_{\kappa} \simeq 550$  fs and an associated Purcell factor of  $> 10^6$ . This rate enhancement of the spontaneous emission of antenna-coupled molecular vibrations opens new avenues for IR coherent control, quantum information processing, and quantum chemistry.

DOI: [10.1103/PhysRevLett.123.153001](https://doi.org/10.1103/PhysRevLett.123.153001)

IR spectroscopy plays a key role for chemical analysis because of its high sensitivity to molecular structure, intramolecular and intermolecular coupling, and molecular dynamics. However, the mode mismatch between atomic scale dimensions of chemical bonds and the long wavelength of IR radiation limits the coupling rate between IR field and molecular vibrational quantum states [1,2]. In addition, nonradiative picosecond scale intramolecular relaxation generally restricts IR spectroscopy to absorption with negligible photoluminescence.

However, spontaneous emission is not an intrinsic property of an emitter. Modification of the local density of states (LDOS) through coupling to, e.g., a resonant cavity allows for control of the spontaneous emission rate, as routinely applied in photoluminescence at visible to near-IR frequencies [3–11]. In the mid-IR, plasmonic antennas have been utilized for increasing spectroscopic sensitivity in surface enhanced IR absorption [12–14]. Yet, only coherent time-domain and multidimensional spectroscopies so far have provided preliminary evidence of a faster antenna-coupled vibrational dephasing. However, the multiple optical interactions in nonlinear spectroscopies make the deconvolution into elementary signal contributions difficult [15–17].

IR scattering scanning near-field optical microscopy (*s*-SNOM) offers a new route for spectroscopic and time-resolved measurements of small molecular ensembles coupled to a single IR dipole antenna. Conventionally, most near-field measurements have focused on a frequency domain analysis that is largely insensitive to variations in vibrational lifetime caused by a modification in the LDOS, because of convoluted spectra arising from Fano interference [18].

Here we show rate enhancement of spontaneous emission of molecular vibrations when resonantly coupled to IR antennas using time-domain IR *s*-SNOM nanoimaging. With the *s*-SNOM tip in weak near-field interaction with the antenna, we locally probe the antenna-coupled molecular vibrations [19,20]. Similar to time-domain nuclear magnetic resonance (NMR), we measure and analyze the vibrational free-induction decay (FID), which allows us to extract the transverse dephasing time  $T_{2,\text{vib}}$  and its modification. When tuning the antenna across a molecular resonance, we observe an up to 50% decrease in vibrational dephasing time  $T_{2,\text{vib}}$ . As the transverse and longitudinal relaxation times are related via the relation  $1/T_{2,\text{vib}} = 1/2T_{1,\text{vib}} + 1/T_{2,\text{vib}}^*$ , and pure dephasing of the molecular vibrations described by  $T_{2,\text{vib}}^*$  is not affected by antenna resonance tuning, we attribute the measured modification in dephasing time  $T_{2,\text{vib}}$  to an enhancement in the LDOS that causes an increased population decay of the molecular vibrations governed by the longitudinal relaxation time  $T_{1,\text{vib}}$ . Fitting a coupled oscillator model quantifies the underlying ultrafast coupling-induced decay time of  $T_{\kappa} \approx 550$  fs, which corresponds to a Purcell factor of  $> 10^6$ .

Figure 1(a) illustrates the relevant relaxation pathways of IR antenna-coupled molecular vibrations. IR antennas couple efficiently to the far field with a radiative lifetime  $T_{1,\text{ant}}^{\text{rad}}$  of typically a few to up to several tens of femtoseconds, competing against the Drude damping ( $T_{2,\text{ant}}^{\text{rad}}$ ) of typically  $\sim 10$ – $30$  fs for Au or Ag [21–25]. In contrast, the vibrational lifetime of condensed phase molecular vibrations is dominated by nonradiative relaxation on timescales  $T_{2,\text{vib}}^{\text{rad}}$  of hundreds of femtoseconds caused by intramolecular vibrational redistribution (IVR), which strongly dominates over the microsecond to millisecond IR spontaneous

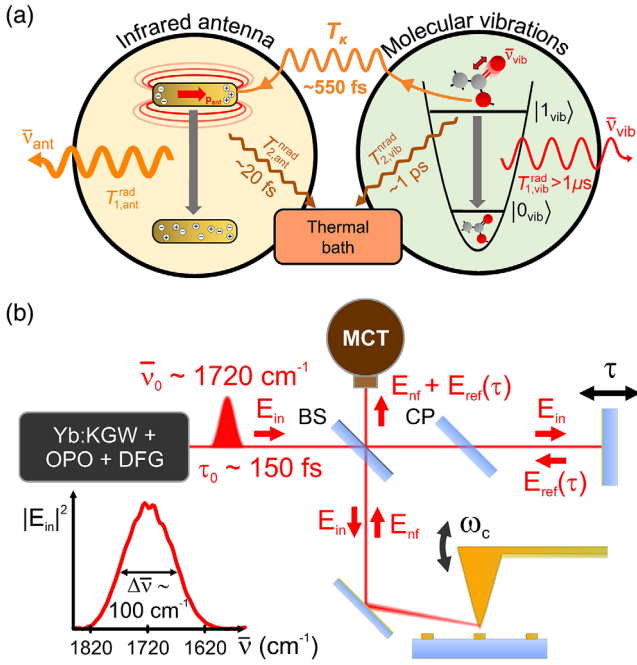


FIG. 1. (a) Timescales of radiative (rad) and nonradiative (nrad) relaxation pathways of IR antenna-coupled molecular vibrations that are measured by nanolocalized time-domain free-induction decay IR *s*-SNOM imaging. (b) Experimental setup for IR pulse generation using optical parametric oscillator (OPO) and difference frequency generation (DFG), shown with interferometric heterodyne detection scheme (BS, beam splitter; CP, compensation plate; MCT, mercury cadmium telluride detector;  $E_{in}$ , incident field;  $E_{ref}$ , reference field;  $E_{nf}$ , tip-scattered near field;  $\omega_c$ , tapping frequency).

emission  $T_{1,vib}^{rad}$  [26–29]. Yet, when molecular vibrations are coupled to the enhanced electromagnetic LDOS of a resonant IR antenna, an increased population decay of the molecular vibrations should be observed as soon as the antenna-molecule coupling time  $T_{\kappa}$  becomes comparable to the intrinsic vibrational nonradiative relaxation  $T_{2,vib}^{nrad}$  [see Fig. 1(a)]. This would manifest itself in a decrease in the coupled vibrational dephasing time controllable through antenna resonance tuning.

For direct time domain IR *s*-SNOM measurements as shown in Fig. 1(b), femtosecond IR radiation is focused onto the molecule-covered antenna, with asymmetric interferometric heterodyne detection and amplification of the nanolocalized tip-scattered near field  $E_{nf}$  with the time-delayed reference field  $E_{ref}(\tau)$ . The resulting asymmetric FID  $I_{FID}(\tau)$  of the near-field response then contains the vibrational dynamic information and the Fourier transformation analogue of the nanoscale dispersion and absorption  $A$  [30–35]. As established previously [20], the tip does not significantly influence the antenna-molecule coupled dynamics itself for a bright mode of an antenna, as is the case here. It merely provides for subdiffraction-limited nanolocalized excitation and detection at the

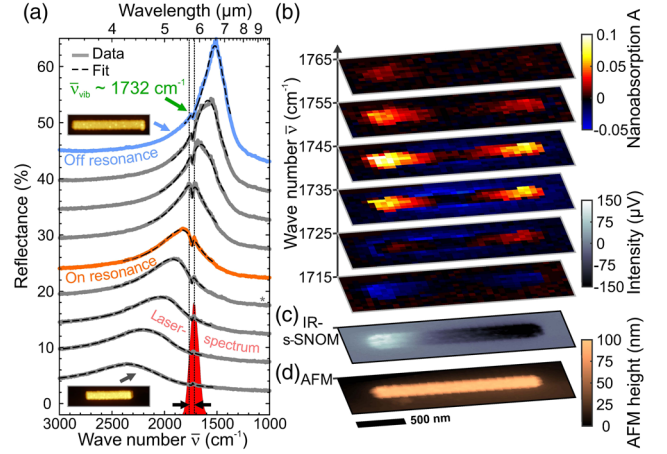


FIG. 2. (a) Measured reflectance spectra of PMMA-covered IR antenna arrays, with increasing antenna length from  $1.3$  to  $2.1$   $\mu m$  from bottom to top, with a nominal step size of  $100$  nm (stacked by  $5\%$  increments). (b) Spatio-spectral nanoimaging of the nanoscale absorption  $A$  for a single IR antenna, with spectrum indicated by the asterisk in (a) and in the spectral range indicated by the two black arrows in (a), revealing enhanced molecular absorption centered at the antenna terminals, (c) near-field intensity, and (d) AFM height of a single PMMA-covered IR antenna.

antenna terminals to probe the resonant antenna-molecule coupling.

Figure 2(a) shows ensemble reflectance spectra of gold IR antenna arrays on a  $CaF_2$  substrate after spin coating a  $10$  nm thin film of poly(methylmethacrylate) (PMMA). The spectra are dominated by a Lorentzian antenna response, while the resonant coupling to the carbonyl stretch mode in PMMA at  $1732$   $cm^{-1}$  manifests itself as a detuning-dependent asymmetric Fano line shape [36,37]. We then perform spatio-spectral nanoimaging of individual PMMA-covered antennas. FID signals of the molecular vibrational response are measured in a spatial grid over the antenna, and are Fourier transformed and normalized with respect to a gold reference substrate. A resulting spatio-spectral image of the nanoscale absorption  $A = \text{Im}\{I_{FID,ant}(\nu)/I_{FID,Au}(\nu)\}$  is shown in Fig. 2(b). We find spatially and spectrally localized molecular resonant enhancement at the antenna terminals at  $\sim 1732$   $cm^{-1}$  as expected [38]. For comparison Figs. 2(c) and 2(d) show a spectrally integrated IR *s*-SNOM image and an atomic force microscopy (AFM) image, respectively.

To investigate the underlying ultrafast dynamics, we analyze the FID traces in the time domain measured with the tip positioned in the near-field region above one of the two antenna terminals, so that the IR antenna mode is most efficiently coupled into the far field. Figures 3(a) and 3(b) show *s*-SNOM FID signals of a resonant [red, Fig. 3(a)] and an off-resonant [blue, Fig. 3(b)] IR antenna [correspondingly colored far-field spectra; see Fig. 2(a)]. The symmetric signal between  $-0.3$  and  $+0.3$  ps is dominated by an off-resonant background and the IR antenna response

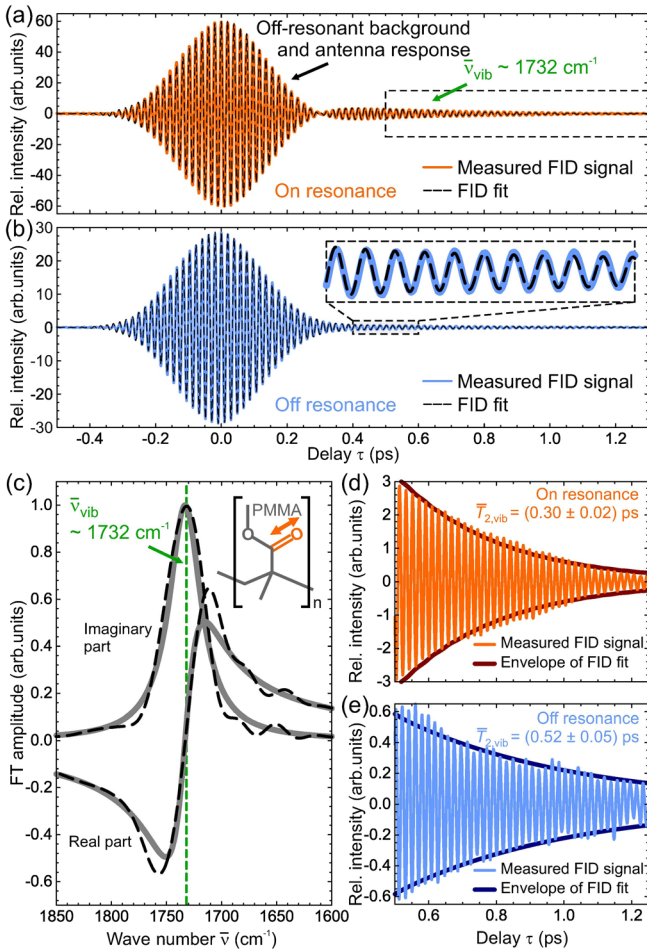


FIG. 3. Measured FID signals of small molecular ensembles coupled to a resonant (a) and an off-resonant (b) IR antenna, together with time-domain fits using Eq. (1). (c) Normalized real and imaginary  $s$ -SNOM spectra from Fourier transform of (a). (d),(e) Enlargement of the vibrational tails of the FID signals from (a) and (b), together with the amplitude envelope of the fit. The vibrational signal from the resonant antenna is roughly 5 times larger than that from the off-resonant antenna.

of few-femtosecond dynamics. For delays  $\tau > 0.5$  ps, only the longer-lived molecular vibrations contribute to the asymmetric FID tail. The corresponding Fourier transform shows the real and imaginary spectra [Fig. 3(c)] with a typical dispersive and absorptive line shape at the carbonyl stretching mode ( $\bar{\nu}_{\text{vib}} \sim 1732 \text{ cm}^{-1}$ ). The broad linewidth of  $\sim 50 \text{ cm}^{-1}$  already indicates an accelerated dephasing of the antenna-coupled molecular vibrations. Therefore, the temporally separated resonant molecular response allows us to directly analyze the modification in vibrational dephasing. Figure 3(d), with an enlargement of the FID tail of the vibrational resonant signal from Fig. 3(a), already qualitatively shows the faster dephasing, and an about 5 times higher signal as compared to the off-resonant case in Fig. 3(e).

For a detailed analysis we describe the heterodyne term of the FID signal  $I_{\text{FID}}(\tau)$  by

$$I_{\text{FID}}(\tau) \propto \int_{-\infty}^{+\infty} E_{\text{nf}}(t) E_{\text{ref}}^*(t - \tau) dt, \quad (1)$$

where  $E_{\text{nf}}$  and  $E_{\text{ref}}$  are the tip-scattered near field and the reference field, respectively.

While  $E_{\text{ref}}(\tau)$  corresponds to the incident laser field  $E_{\text{in}}$  (with delay  $\tau$ ), the tip-scattered near field  $E_{\text{nf}}$  is modified by the antenna response  $g_{\text{ant}}(t)$ , as well as by the coupled response function  $\bar{g}_{\text{vib}}(t)$  of the molecular vibrations, with the overbar indicating the coupling-induced modification of the molecular dynamics. Without the *a priori* knowledge of coupling, we express  $E_{\text{nf}}(t)$  in the time domain as a sum of these two contributions as

$$E_{\text{nf}}(t) \propto a_{\text{ant}} e^{i\phi_{\text{ant}}} \int_{-\infty}^{+\infty} g_{\text{ant}}(t - t') E_{\text{in}}(t') dt' + \bar{a}_{\text{vib}} e^{i\bar{\phi}_{\text{vib}}} \int_{-\infty}^{+\infty} \bar{g}_{\text{vib}}(t - t') E_{\text{in}}(t') dt', \quad (2)$$

where we accounted for the different amplitudes  $a_{\text{ant}}$  and  $\bar{a}_{\text{vib}}$  and phases  $\phi_{\text{ant}}$  and  $\bar{\phi}_{\text{vib}}$  of the antenna and the molecular response, respectively.

The antenna response function  $g_{\text{ant}}(t)$  is treated as almost instantaneous (see Supplemental Material [39]), since in the spectral domain it varies little over the bandwidth of our laser spectrum [see Fig. 2(a)]. The response of the molecular vibrations  $\bar{g}_{\text{vib}}(t)$  is modeled as a harmonic oscillator with resonance frequency  $\bar{\omega}'_{\text{vib}}$  and dephasing time  $\bar{T}_{2,\text{vib}}$ :

$$\bar{g}_{\text{vib}}(t) = \frac{i}{2\bar{\omega}'_{\text{vib}}} e^{-t/\bar{T}_{2,\text{vib}}} e^{-i\bar{\omega}'_{\text{vib}} t} \theta(t), \quad (3)$$

with  $\theta(t)$  being the Heaviside distribution.

We now use  $\bar{\omega}'_{\text{vib}}$ ,  $\bar{T}_{2,\text{vib}}$ , the amplitudes  $a_{\text{ant}}$  and  $\bar{a}_{\text{vib}}$ , the phases  $\phi_{\text{ant}}$  and  $\bar{\phi}_{\text{vib}}$ , and the antenna response with free parameters to fit the measured FID signals with Eq. (1). The result of two examples is shown in Fig. 3, where we find the experimental FID traces in good agreement with this model fit for values of  $\bar{T}_{2,\text{vib}} = (0.30 \pm 0.02) \text{ ps}$  and  $\bar{T}_{2,\text{vib}} = (0.52 \pm 0.05) \text{ ps}$  for the resonant [Fig. 3(a), 3(d)] and the off-resonant [Fig. 3(b), 3(e)] case, respectively.

In order to further analyze the variation of vibrational dephasing as a function of antenna resonance, we perform a series of measurements, with five measurements each, for different antennas of nominally identical resonance frequency. The extracted vibrational dephasing times  $\bar{T}_{2,\text{vib}}$ , the normalized vibrational amplitudes  $\bar{a}_{\text{vib}} = \bar{a}_{\text{vib}}/a_{\text{ant}}$ , and phases  $\Delta\phi = \bar{\phi}_{\text{vib}} - \phi_{\text{ant}}$  are shown in Figs. 4(a)–4(c) as a function of the antenna resonance  $\nu_{\text{ant}}$ . Already from qualitative inspection we find a pronounced minimum in the dephasing time  $\bar{T}_{2,\text{vib}}$  when the antenna is on resonance with the molecular vibration [Fig. 4(a)]. Associated is a peak in the vibrational signal amplitude  $\bar{a}_{\text{vib}}$  [Fig. 4(b)], and the phase of the molecular oscillators  $\Delta\phi$  changes

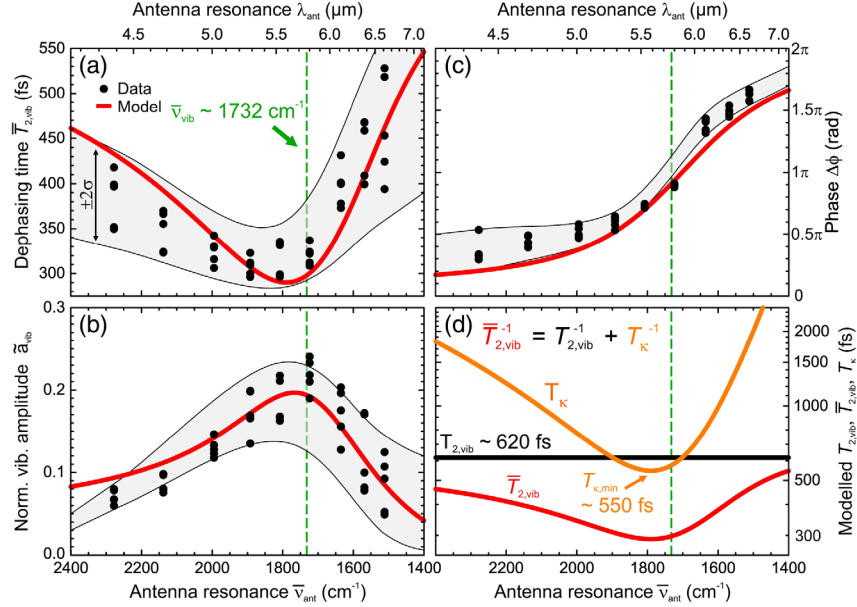


FIG. 4. (a) Measured vibrational dephasing time  $\bar{T}_{2,\text{vib}}$ , (b) vibrational amplitude  $\tilde{a}_{\text{vib}}$ , and (c) phase  $\Delta\phi$  as a function of antenna resonance  $\bar{\nu}_{\text{ant}}$ . The gray areas indicate the standard deviation  $\pm 2\sigma$ . The solid red lines are fits to the coupled oscillator model. (d) Deconvolution of the modeled dephasing time  $\bar{T}_{2,\text{vib}}(\nu_{\text{ant}})$ , into unperturbed dephasing time  $T_{2,\text{vib}}$  and coupling-induced population decay time  $T_{\kappa}$ , with  $\bar{T}_{2,\text{vib}}^{-1} = T_{2,\text{vib}}^{-1} + T_{\kappa}^{-1}$ .

monotonically by almost  $2\pi$  across the tuning range of the IR antennas [Fig. 4(c)].

We model the combined dynamics of antenna and molecules as coupled harmonic oscillators, where the effective amplitude of the IR antenna  $x_{\text{ant}}(t)$  and the molecular oscillators  $x_{\text{vib}}(t)$  is coupled by a phenomenological coupling constant  $\kappa$ :

$$\ddot{x}_{\text{ant}} + 2/T_{2,\text{ant}}\dot{x}_{\text{ant}} + \omega_{\text{ant}}^2 x_{\text{ant}} - \kappa x_{\text{vib}} = qE_{\text{in}}(t), \quad (4)$$

$$\ddot{x}_{\text{vib}} + 2/T_{2,\text{vib}}\dot{x}_{\text{vib}} + \omega_{\text{vib}}^2 x_{\text{vib}} - \kappa x_{\text{ant}} = 0. \quad (5)$$

$T_{2,\text{ant}}$  and  $T_{2,\text{vib}}$  and  $\omega_{\text{ant}}$  and  $\omega_{\text{vib}}$  are the uncoupled dephasing times and resonance frequencies, respectively, and  $q$  describes the excitation strength of the IR antenna. As is apparent from Eqs. (4) and (5), we assume that only the IR antenna is excited by the incident field  $E_{\text{in}}$ , and the molecular vibrations are only excited through the IR antenna; i.e., we neglect direct tip-induced vibrational excitation [20]. The phenomenological coupling constant  $\kappa$  accounts for the combined effects of near-field and radiative coupling [40].

Solving the coupled differential equations (4) and (5), in the case of weak coupling, leads to eigenmodes with new eigenfrequencies  $\bar{\omega}_{\text{ant}}$  and  $\bar{\omega}_{\text{vib}}$ , and modified dephasing times  $\bar{T}_{2,\text{ant}}$  and  $\bar{T}_{2,\text{vib}}$ , and yields the vibrational amplitude  $\tilde{a}_{\text{vib}}$  and phase  $\Delta\phi$ . For the coupled vibrational dephasing time  $\bar{T}_{2,\text{vib}}$  we find to a good approximation (for results of the vibrational amplitude  $\tilde{a}$  and phase  $\Delta\phi$ , see Supplemental Material [39])

$$\frac{1}{\bar{T}_{2,\text{vib}}} = \frac{1}{T_{2,\text{vib}}} - \underbrace{\frac{\kappa^2}{4\omega'_{\text{ant}}\omega'_{\text{vib}}\Delta\omega'^2 + \Delta\Gamma^2}}_{1/T_{\kappa}}, \quad (6)$$

with  $\omega'_i = \omega_i^2 - 1/T_{2,i}^2$  ( $i = \text{ant}, \text{vib}$ ) the redshifted near-field resonance frequencies of the IR antenna and the molecular oscillators [41–43],  $\Delta\Gamma = 1/T_{2,\text{vib}} - 1/T_{2,\text{ant}}$  the difference in the dephasing rate, and the detuning  $\Delta\omega' = \omega'_{\text{vib}} - \omega'_{\text{ant}}$ .

Equation (6) shows the effect of the coupling-induced population decay time  $T_{\kappa}$ , which accounts for damping of the molecular vibrations through the IR antenna. In the bad cavity regime, i.e.,  $T_{2,\text{ant}} < T_{2,\text{vib}}$ , as is the case for our experiments,  $T_{\kappa}$  is positive, and polarization transfer from the molecules toward the antenna dominates over the reverse process [44].

We then use the model to simultaneously fit the antenna resonance dependence of the measured vibrational dephasing time  $\bar{T}_{2,\text{vib}}$ , the vibrational amplitude  $\tilde{a}_{\text{vib}}$ , and phase  $\Delta\phi$ , as shown in Figs. 4(a)–4(c). The model not only captures the dip and spectral asymmetry in the dephasing time  $\bar{T}_{2,\text{vib}}$  and the amplitude  $\tilde{a}_{\text{vib}}$ , but also describes the phase variation  $\Delta\phi$  correctly. The reason for the  $2\pi$  phase change, rather than  $\pi$  as in case of a normal resonance, is that the molecular vibrations not only emit to but are also excited through the IR antenna. Notably, as the IR *s*-SNOM tip is not taken into account in our model, the good agreement between measurement and model supports the

fact that the off-resonant coupling of the tip does not affect the vibrational dynamics itself.

In Fig. 4(d) we show the deconvolution, i.e., the individual contributions to the relaxation pathways of the molecular excitations as extracted from the oscillator model. For the uncoupled intrinsic vibrational dephasing time  $T_{2,\text{vib}}$ , we find a value of  $\sim 620$  fs, mostly originating from IVR dephasing, contributing to net absorption dissipated as heat. Yet, the antenna-coupled vibrational dephasing time  $\bar{T}_{2,\text{vib}}$  varies between the off-resonant limit given by  $T_{2,\text{vib}} \sim 620$  fs and a minimum of  $\sim 300$  fs for resonant coupling. This is a manifestation of the coupling-induced modification of the vibrational relaxation time  $T_x$  through the IR antenna, which over the tuning range of the experiment varies between  $\sim 1.5$  ps and  $\sim 550$  fs. This variation of the ratio of inherent nonradiative decay vs coupling-induced population decay through the IR antenna between 1:3 and 1:1 is consistent with the corresponding normalized vibrational amplitude increase by a factor of  $\sim 2$  [see Fig. 4(b)]. Note that the amplitude enhancement factor does not represent the Purcell factor, as observed *s*-SNOM signals are already enhanced through the AFM tip and convolved with different phase-sensitive contributions in addition to the antenna-coupled rate enhancement of the molecular spontaneous emission.

The spectral variation of the vibrational dephasing time is a clear signature for a new relaxation pathway for the molecular vibrations, with sub-picosecond unidirectional coherent vibrational near-field energy transfer to the IR antenna. Subsequently, the ratio of radiative and nonradiative relaxation pathways of the antenna determines the fraction of vibrational energy dissipated as heat by Drude damping or radiated to the far field [24,45]. As the intrinsic lifetime for spontaneous emission of molecular vibrations is as long as microseconds to milliseconds [26–29], the rate enhancement of the spontaneous emission into the IR antenna corresponds to a Purcell factor of  $>10^6$ .

In summary, our results contribute to a deeper understanding of molecule-antenna coupling and associated dynamics of competing relaxation pathways with immediate implications for analytical surface enhanced IR absorption and ultrafast vibrational spectroscopy. They further provide insight into the ultrafast time scales underlying the formation of new hybrid IR vibrational light-matter states [46]. Our findings enable a range of applications, from molecular quantum optics with single IR photon emitters to IR coherent control for novel forms of vibrational photochemistry.

We thank Eric Ellison for support with far-field sample characterization, and Vasily Kravtsov, Ana Maria Rey, and Mathew Pelton for helpful discussions. We acknowledge funding from the NSF Science and Technology Center on Real-Time Functional Imaging (STROBE) under DMR-1548924, and a QuEST award from the University of Colorado, and the ERC (ComplexPLAS).

\*markus.raschke@colorado.edu

- [1] S. L. Baughcum and S. R. Leone, *J. Chem. Phys.* **72**, 6531 (1980).
- [2] J. D. Jackson, *Classical Electrodynamics*, 3rd ed. (Wiley, New York, 1998).
- [3] J. M. Gérard, B. Sermage, B. Gayral, B. Legrand, E. Costard, and V. Thierry-Mieg, *Phys. Rev. Lett.* **81**, 1110 (1998).
- [4] S. Kühn, U. Håkanson, L. Rogobete, and V. Sandoghdar, *Phys. Rev. Lett.* **97**, 017402 (2006).
- [5] P. Anger, P. Bharadwaj, and L. Novotny, *Phys. Rev. Lett.* **96**, 113002 (2006).
- [6] V. S. C. Manga Rao and S. Hughes, *Phys. Rev. B* **75**, 205437 (2007).
- [7] M. Frimmer, Y. Chen, and A. F. Koenderink, *Phys. Rev. Lett.* **107**, 123602 (2011).
- [8] T. Nakamura, T. Asano, K. Kojima, T. Kojima, and S. Noda, *Phys. Rev. B* **84**, 245309 (2011).
- [9] R. Albrecht, A. Bommer, C. Deutsch, J. Reichel, and C. Becher, *Phys. Rev. Lett.* **110**, 243602 (2013).
- [10] G. M. Akselrod, C. Argyropoulos, T. B. Hoang, C. Ciraci, C. Fang, J. Huang, D. R. Smith, and M. H. Mikkelsen, *Nat. Photonics* **8**, 835 (2014).
- [11] H. Kaupp, T. Hümmer, M. Mader, B. Schleder, J. Benedikter, P. Haeusser, H.-C. Chang, H. Fedder, T. W. Hänsch, and D. Hunger, *Phys. Rev. Applied* **6**, 054010 (2016).
- [12] F. Neubrech, A. Pucci, T. W. Cornelius, S. Karim, A. García-Etxarri, and J. Aizpurua, *Phys. Rev. Lett.* **101**, 157403 (2008).
- [13] R. Adato, A. A. Yanik, J. J. Amsden, D. L. Kaplan, F. G. Omenetto, M. K. Hong, S. Erramilli, and H. Altug, *Proc. Natl. Acad. Sci. U.S.A.* **106**, 19227 (2009).
- [14] F. Neubrech, C. Huck, K. Weber, A. Pucci, and H. Giessen, *Chem. Rev.* **117**, 5110 (2017).
- [15] O. Selig, R. Siffels, and Y. L. A. Rezus, *Phys. Rev. Lett.* **114**, 233004 (2015).
- [16] J. P. Kraack, A. Frei, R. Alberto, and P. Hamm, *J. Phys. Chem. Lett.* **8**, 2489 (2017).
- [17] B. Xiang, R. F. Ribeiro, A. D. Dunkelberger, J. Wang, Y. Li, B. S. Simpkins, J. C. Owrutsky, J. Yuen-Zhou, and W. Xiong, *Proc. Natl. Acad. Sci. U.S.A.* **115**, 4845 (2018).
- [18] D. Dregely, F. Neubrech, H. Duan, R. Vogelgesang, and H. Giessen, *Nat. Commun.* **4**, 2237 (2013).
- [19] R. L. Olmon, M. Rang, P. M. Krenz, B. A. Lail, L. V. Saraf, G. D. Boreman, and M. B. Raschke, *Phys. Rev. Lett.* **105**, 167403 (2010).
- [20] E. A. Muller, B. Pollard, H. A. Bechtel, R. Adato, H. Altug, and M. B. Raschke, *ACS Photonics* **5**, 3594 (2018).
- [21] C. Sönnichsen, T. Franzl, T. Wilk, G. von Plessen, J. Feldmann, O. Wilson, and P. Mulvaney, *Phys. Rev. Lett.* **88**, 077402 (2002).
- [22] R. Adato, A. A. Yanik, C.-H. Wu, G. Shvets, and H. Altug, *Opt. Express* **18**, 4526 (2010).
- [23] T. Hanke, J. Cesar, V. Knittel, A. Trügler, U. Hohenester, A. Leitenstorfer, and R. Bratschitsch, *Nano Lett.* **12**, 992 (2012).
- [24] V. Kravtsov, S. Berweger, J. M. Atkin, and M. B. Raschke, *Nano Lett.* **14**, 5270 (2014).

- [25] T. Neuman, C. Huck, J. Vogt, F. Neubrech, R. Hillenbrand, J. Aizpurua, and A. Pucci, *J. Phys. Chem. C* **119**, 26652 (2015).
- [26] L. Allen and J. H. Eberly, *Optical Resonance and Two-Level Atoms* (John Wiley and Sons, Inc., New York, 1975).
- [27] Q. Shi and E. Geva, *J. Phys. Chem. A* **107**, 9059 (2003).
- [28] M. Fox, *Quantum Optics: An Introduction* (Oxford University Press, Oxford, 2006).
- [29] L. Chen, J. A. Lau, D. Schwarzer, J. Meyer, V. B. Verma, and A. M. Wodtke, *Science* **363**, 158 (2019).
- [30] S. Amarie, T. Ganz, and F. Keilmann, *Opt. Express* **17**, 21794 (2009).
- [31] M. Schnell, A. Garcia-Etxarri, A. J. Huber, K. B. Crozier, A. Borisov, J. Aizpurua, and R. Hillenbrand, *J. Phys. Chem. C* **114**, 7341 (2010).
- [32] X. G. Xu, M. Rang, I. M. Craig, and M. B. Raschke, *J. Phys. Chem. Lett.* **3**, 1836 (2012).
- [33] F. Huth, A. Govyadinov, S. Amarie, W. Nuansing, F. Keilmann, and R. Hillenbrand, *Nano Lett.* **12**, 3973 (2012).
- [34] I. Amenabar, S. Poly, W. Nuansing, E. H. Hubrich, A. A. Govyadinov, F. Huth, R. Krutokhvostov, L. Zhang, M. Knez, J. Heberle, A. M. Bittner, and R. Hillenbrand, *Nat. Commun.* **4**, 2890 (2013).
- [35] E. A. Muller, B. Pollard, and M. B. Raschke, *J. Phys. Chem. Lett.* **6**, 1275 (2015).
- [36] N. Liu, L. Langguth, T. Weiss, J. Kästel, M. Fleischhauer, T. Pfau, and H. Giessen, *Nat. Mater.* **8**, 758 (2009).
- [37] B. Luk'yanchuk, N. I. Zheludev, S. A. Maier, N. J. Halas, P. Nordlander, H. Giessen, and C. T. Chong, *Nat. Mater.* **9**, 707 (2010).
- [38] B. Pollard, E. A. Muller, K. Hinrichs, and M. B. Raschke, *Nat. Commun.* **5**, 3587 (2014).
- [39] See Supplemental Material at <http://link.aps.org/supplemental/10.1103/PhysRevLett.123.153001> for a detailed solution of the coupled oscillator model.
- [40] A. Gandman, R. T. Mackin, B. Cohn, I. V. Rubtsov, and L. Chuntanov, *ACS Nano* **12**, 4521 (2018).
- [41] J. Zuloaga and P. Nordlander, *Nano Lett.* **11**, 1280 (2011).
- [42] B. Metzger, M. Hentschel, M. Lippitz, and H. Giessen, *Opt. Lett.* **37**, 4741 (2012).
- [43] P. Alonso-González, P. Albella, F. Neubrech, C. Huck, J. Chen, F. Golmar, F. Casanova, L. E. Hueso, A. Pucci, J. Aizpurua, and R. Hillenbrand, *Phys. Rev. Lett.* **110**, 203902 (2013).
- [44] P. Torma and W. L. Barnes, *Rep. Prog. Phys.* **78**, 013901 (2015).
- [45] M. B. Raschke, S. Berweger, and J. M. Atkin, in *Plasmonics: Theory and Applications*, edited by T. V. Shahbazyan and M. I. Stockman (Springer, New York, 2013), Chap. 7, pp. 237–281.
- [46] A. Thomas, L. Lethuillier-Karl, K. Nagarajan, R. M. A. Vergauwe, J. George, T. Chervy, A. Shalabney, E. Devaux, C. Genet, J. Moran, and T. W. Ebbesen, *Science*, **363**, 615 (2019).